The Effects of a Flexible, Flapping Airfoil on Power Extraction and Propulsive Efficiency: A Numerical Solution

Joseph A. O'Gara[1]

University of New South Wales at the Australian Defence Force Academy

The use of pitching, plunging airfoils for both propulsion and power extraction in recent history has gained much interest due to its relatively high efficiencies at low Reynolds numbers. Chordwise airfoil flexibility has been shown to increase the efficiency of both flapping propulsion and power extraction, however research into the passive deformation of such an airfoil under aerodynamic load is minimal. A method was developed in order to allow the quasi two-dimensional testing of a pitching, plunging airfoil for both power extraction and propulsion. By utilising Computational Fluid Dynamics and Finite Element Analysis software, Fluid Structure Interaction was achieved enabling calculation of the aeroelastic deformation of a flapping cycle under both aerodynamic and inertial loads. It was found that for flapping wing propulsion, there is an exponential relationship between increases of propulsive efficiency and increasing airfoil flexibility.

Contents

I. Background 2
II. Airfoil Motion Kinematics 3
A. Power Extraction 3
B. Propulsion 4
III. Performance Measures 4
A. Power Extraction 4
B. Propulsion 4
IV. Computational Approach 5
A. General 5
B. Fluid Solver 5
C. Structural Solver 7
D. Flexibility 7
E. Convergence 7
V. Validation 7
VI. Results 9
VII. Conclusion 11
VIII. Recommendations 11
Acknowledgements 12
References 12

[1] *Pilot Officer*, School of Engineering & Information Technology. ZEIT4500

Nomenclature

c	Chord length (m)	T	Time period (s)
d	Total Vertical Displacement	U_∞	Freestream Velocity (m/s)
f	Flapping Frequency (1/T)	V_y	Heaving Velocity (m/s)
f^*	Non-Dimensional Frequency (fc/U_∞)	α	Angle of Attack (deg)
H_0	Heaving amplitude	η	Turbine Efficiency (P/P_A)
h	Vertical Displacement	θ	Pitch Angle about pivot point
k	Reduced Frequency ($2\pi f^*$)	θ_0	Pitch Amplitude (rad)
L	Aerodynamic Lift (N)	ϕ	Phase Difference (rad)
P	Power Extracted from flow (W)	LE	Leading Edge
P_A	Power Available from flow (W)	LEV	Leading Edge Vortices
Re	Reynolds Number ($\frac{\rho U_\infty c}{\mu}$)	TE	Trailing Edge
		TEV	Trailing Edge Vortices
St	Strouhal Number ($\frac{fA}{U}$)	FSI	Fluid Structure Interaction

I. Background

The use of pitching, plunging wings for both power extraction and propulsion is an area of much interest and research since the late 20th century. Conventional wings rely on the steady, laminar flow of a fluid over the wing surface in order to create lift. Flapping wing power and force generators take inspiration from the insect and animal kingdoms by using high angles of attack and sharp vertical, plunging motions in order to create strong low pressure rotating fluid bodies. Known as Leading Edge Vortices or LEVs, these low pressure regions create high instantaneous lift forces which enable power extraction, and sustained forward thrust forces which can be used for propulsion. This technique can produce relatively high forces at relatively low Reynolds numbers.

The modern study of flapping wing airfoil designs for both power extraction and thrust generation was ignited by researchers McKinney and DaLaurier [9] who in 1980 investigated the potential of an oscillating airfoil for the extracting of wind energy. They concluded that the extraction of power with a flapping airfoil was a feasible one, even remarking at the unexpectedly high efficiencies achieved. Since then there has been a resurgence of research into this field.

Conventional power generation is limited by Betz's Limit which states that maximum power that can be extracted from the kinetic energy of a fluid is 59.3%. Modern day turbines can achieve approximately 70-80% of this theoretical limit, or roughly 45% of the total power available. It has been shown previously by the work of Kinsey and Dumas [4] and others, that flapping wing power extraction is capable of efficiencies of approximately 50% in a dual tandem flapping extraction cycle.

Previous research into the shape, size and path of the airfoil used in flapping power generation has shown that both motion related features and the overall shape of the airfoil have the ability to improve efficiency of power extraction. Work done by both Kinsey and Dumas [5] and Ashraf [1] have suggested that the thickness and hence shape of the airfoil does effect the efficiency of power extraction. Work done by Le *et al.* [6] have also looked into natural shapes such as scallop shape, mimicking the shape of dragon fly wings with camber to increase efficiency.

Much interest has been raised recently, particularly in the last decade, about the use of chordwise flexible airfoils for use in Micro Air Vehicles. Both passively deforming airfoils (that deform under aerodynamic load - known as aeroelastics) and active deformation (involving prescribed airfoil deformation) has been researched somewhat extensively. Research by Hoke *et al.* [3] and Lui *et al.* [7] has also shown that varying the shape of the airfoil at certain time steps within the flapping cycle can increase the power extraction efficiency. Work in this area has been promising with efficiency increases of up to 16% [3].

The aims of this project are centralized around the development and implementation of methodology that can be used to allow the simulation of a pitching, plunging airfoil for power extraction using Fluid Structure Interaction. The propulsive regime however proved vital in allowing the verification of methods used and the validation of results due the larger body of works about the area. The propulsive case was found to be greatly less difficult to setup and many times faster to simulate. Thus propulsive results are used within this body of work to validate the methodology for the power extraction regime, whilst at the same time allowing the discussion of how propulsive efficiency is effected by increased flexibility.

II. Airfoil Motion Kinematics

A. Power Extraction

Kinsey and Dumas [5] in their study of an oscillating airfoil defined the movement of the airfoil by its concurrent pitching $\theta(t)$ motion and heaving motion $h(t)$. This allowed the following equations of motion to be formed:

$$\theta(t) = \theta_0 \sin(\gamma t) \quad (1)$$

$$h(t) = H_0 \sin(\gamma t + \phi) \quad (2)$$

θ_0, H_0 are the pitching and heaving amplitudes, γ denotes angular frequency ($2\pi f$) and ϕ is the phase difference between heaving and pitching motions. Figure 1 illustrates the physical attributes of these flow variables.

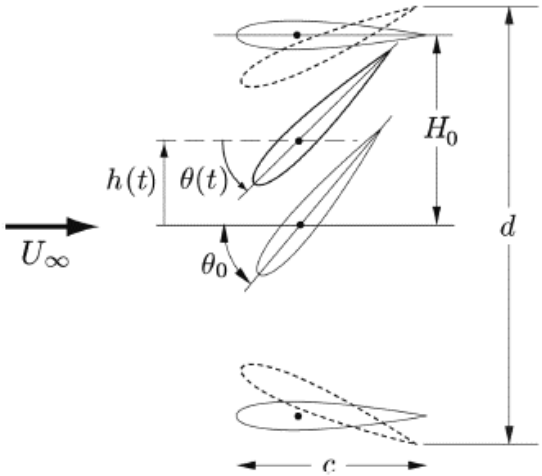

Figure 1 - The motion of a pitching and plunging airfoil about a fixed point – Kinsey and Dumas [5]

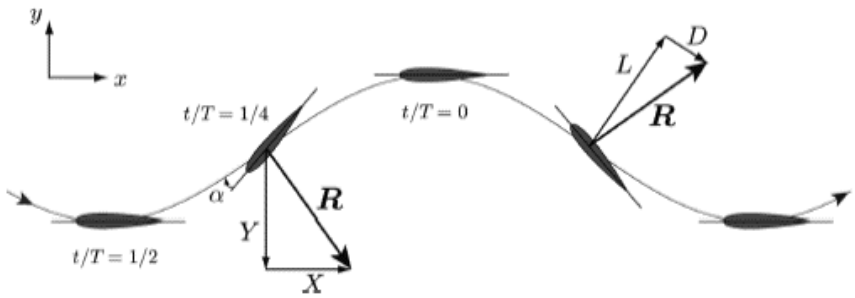

Figure 2 - The motion of a pitching, plunging airfoil over time in a power extraction regime - Kinsey and Dumas [5]

Figure 2 shows the motion of a power extracting airfoil over time. On the right side of this figure, the aerodynamic forces created by the airfoil are shown. These forces are transformed on the left side of the figure into the *X* and *Y* components forces. Therefore for a power extracting airfoil, the *Y* component of the airfoils created forces is in the direction its motion. Thus it can be concluded that there is power being extracted from the flow. It has been shown previously that a phase difference (ϕ) of 90° between pitching and vertical motions is ideal for power extraction [5].

The numerical solutions run for this project will be conducted using simple sinusoidal motion with a non-dimensional frequency (f^*) of 0.14 and maximum pitch angle (θ_0) of 76.33° with a Reynolds number of 1100. A phase angle of 90° will be used. This is consistent with work completed by Kinsey and Dumas [5] and Ashraf *et al.* [1] and will allow comparison of computed results with their work in order to validate results. The airfoil's pivot will be located at the one-third chord.

B. Propulsion

Maio *et al.* [8] and Hoke *et al.* [2] based on Maio's work have both simulated a propulsive regime flapping airfoil through a plunging airfoil with no pitching or rotational motion. Figure 3 shows Maio *et al.*'s setup for their plunging, passively deforming airfoil. In their work, Maio *et al.* chose to locate the pivot point at the leading edge of the airfoil. Hoke does not specify where the pivot location is for his airfoil. In this body of work, the propulsive scheme pivot location is at the one-third chord position.

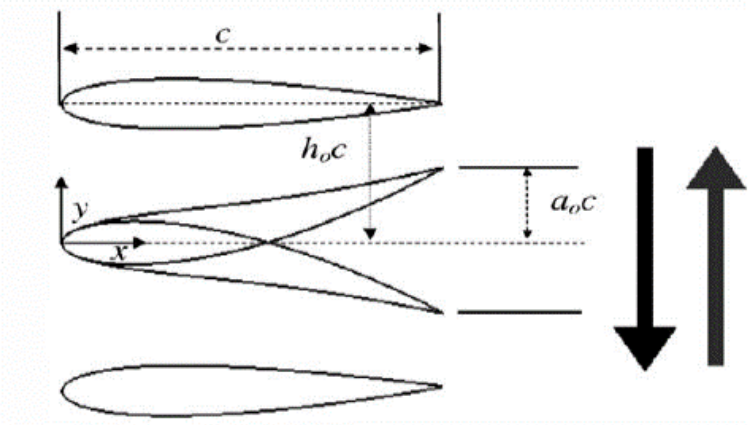

Figure 3 – Airfoil Motion in the Propulsion regime – Maio [8]

Both Maio and Hoke use a reduced frequency of 2 ($k=2$), so in order to allow the validation of results a reduced frequency of 2 was also used for this project. A non-dimensional frequency (f^*) of $\frac{1}{\pi}$ was used.

III. Performance Measures

A. Power Extraction

The efficiency of power extraction, as given by Young *et al.* [10], can be found from the instantaneous and time averaged power coefficient:

$$P = L\dot{y} + M\dot{\theta} \tag{3}$$

$$C_P = \frac{P}{\frac{1}{2}\rho U_\infty^2 sc} = C_L \frac{\dot{y}}{U_\infty} + C_M \frac{\dot{\theta} c}{U_\infty} \tag{4}$$

$$\overline{C_P} = \frac{1}{T}\int_t^{t+T} C_P(t)dt \tag{5}$$

The efficiency is therefore the time averaged power output ($\bar{P}$) divided by the power available (the energy available from the entire flow through the area that the flapping wing sweeps). This is known as "Betz efficiency" and is the same calculation used for finding the efficiency of conventional rotary wind generators.

$$\eta_{extraction} = \frac{\bar{P}}{Pa} = \frac{\bar{P}}{\frac{1}{2}\rho U_\infty^2 sd} = \overline{C_P}\frac{c}{d} \tag{6}$$

B. Propulsion

Propulsive efficiency is a function of time averaged power coefficient (C_P) (Equation 5) and a new time averaged coefficient of thrust. The coefficient of thrust (C_T) is the negative of drag coefficient (C_D). Equations 3-5 allow the calculation of time average power coefficient and Equations 7 can be used to find C_T and hence propulsive efficiency (Equation 8).

$$\bar{C_T} = \frac{1}{T}\int_t^{t+T} -C_D(t)dt \tag{7}$$

$$\eta_{propulsion} = \frac{\bar{C_T}}{\bar{C_P}} \tag{8}$$

IV. Computational Approach

A. General

All simulations are completed using the *ANSYS v14.5* software package. Flexibility of the airfoil is implemented through *ANSYS's* native *System Coupling* capability which allows the linking of the fluid solver *Fluent* and the structural solver *Transient Structural*. Using this process a complete two-way Fluid Structure Interaction, allowing the flow of information (force and displacement) to travel in both directions between the fluid solver and the structural solver.

In order to allow a two-way FSI, the airfoil motion is prescribed in the structural solver through defined motion of the pivot using Equations 1 & 2, which allows the vertical displacement and rotation of the airfoil to be calculated for every time interval. The displacement (motion) of the airfoil is calculated by the structural solver and then supplied to the fluid solver through the *System Coupling* service. Using dynamic meshing, namely 2.5D remeshing, the fluid side mesh is deformed and the flow is calculated to convergence. The pressure acting on the airfoil is then supplied to the structural solver in order to compute the deformation of the airfoil under the perceived aerodynamic load.

The intent of this project is to calculate the effects of flexibility of an airfoil over various motion paths for both propulsion and power extraction. In order to achieve reliable results, a setup which allows for easy comparison to results of researchers such as Kinsey and Dumas [5], Hoke *et al.* [2] and Maio *et al.* [8] is needed. These authors have all studied the two dimensional effects of airfoil shape. However *ANSYS* software limitations dictate that FSI is conducted in 3D. Therefore real 3D effects such as wing tip vortices needed to be negated in order to create comparable results. While 3D effects will be crucial to the performance in the real life implementation of flapping wings, the scope of the project is only wide enough to study one variable relevant to the propulsive and power extracting cases: flexibility. An extruded 2D mesh (shown in Figure 4) was chosen as it allows the flow to be simulated in a quasi two-dimmenstional fashion. This setup entails the use of a one element thick three-dimensional structural and fluid mesh.

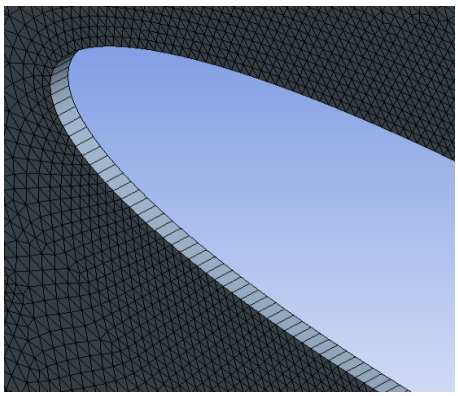

Figure 4 – Fluid Side Extruded 2D Mesh

The power extraction case is ran with a NACA0015 airfoil, whilst a NACA0014 is used for the propuslive case.

B. Fluid Solver

The solution has been calculated using a pressure based three-dimensional Reynolds Averaged Navier Stokes (RANS) model, using laminar, incompressible flow approximations in the transient condition. A Coupled pressure-velocity scheme is used with a Least-Squared Cell Based spatial discretization gradient, a second order pressure term and a second order upwind momentum term. Second order time discretisation is used for the propulsion regime only due to software side limitations when using remeshing.

For both the propulsive and power extraction cases, simulations were run with air of density 1.225 kg/m^3 with a freestream velocity of 1 m/s. Viscosity was adjusted to get the required Reynolds numbers of 1100 and 20,000 for power extraction and propulsive cases respectively.

Figure 5 shows the mesh setup. The left, top and bottom farfield boundaries are specified as velocity inlets and the right farfield is a pressure outlet. The left and right farfield boundaries are located at $X = \pm 20\ m$ and the top and bottom are located at $Y = \pm 20\ m$. Initally, the airfoil pivot location is located at X=0, Y=2m. All mesh elements are extruded triangles, that is, they are 2D triangles, swept, or extruded one element thick.

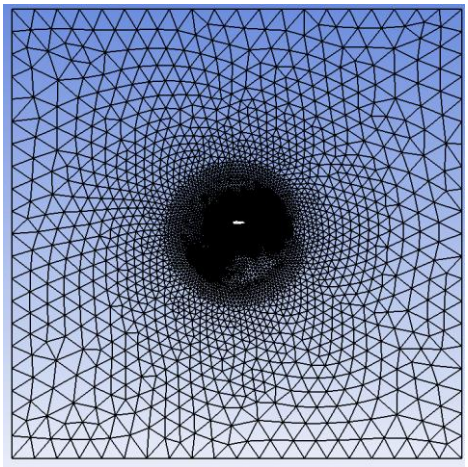

Figure 5 – Mesh Setup

For the propulsive case, as there is minimal rotation of the airfoil through both prescribed motion and pressure deformation, dynamic remeshing through Smoothing only is acceptable. This allows for large timesteps while maintaining a high quality mesh. The propulsive case mesh can therefore be relatively simple. In this case, a high quality mesh is achieved through the specification of the

number of airfoil points and letting the mesh face size grow gradually to the farfield boundary, by setting a relatively small mesh growth rate (1.025 or less). With the use of smoothing the boundary layer mesh is moved with the airfoil, preserving boundary layer mesh quality as the airfoil moves through the mesh.

The mesh setup for the power extraction case is significantly more complex since the smoothing capability in *Fluent* does not cope well with the any sizeable rotation of the airfoil. Without the remeshing of the fluid side mesh, the boundary layer mesh of the airfoil becomes massively distorted due to the large rotational displacement seen. It is important to note that cell orthogonally near the airfoil surface is crucial for the accuracy of results. The ideal boundary layer cells for an unstructured (triangular) mesh such as the one used in this project are equilateral triangles. As visible from Figure 6, the boundary layer mesh has been distorted so that the cells are no longer equilateral as well as they have been noticeably elongated. For visualization purposes a very coarse mesh is pictured in Figure 6, however the same issues are present on a finer mesh. Thus, due to the low quality of mesh produced by large amount of rotation within the mesh, discretization error will be excessively large due to the poor quality of the cells in the boundary layer. Most likely results attained from this method would be incorrect and not able to be validated against results of others. The circled region of the Figure 6 indicates the area of the mesh where the rotation of the mesh can become so large, that negative cell volume was achieved. This means that the one side of the cell essentially twisted over the other side. Negative cell volume will cause the simulation run to crash. Therefore the use of remeshing is crucial in ensuring the quality of the mesh is preserved and the simulation can run reliably.

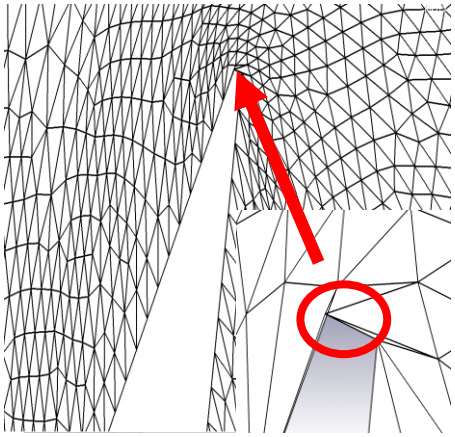

Figure 6 – Skewed Fluid Side Mesh Cells & Negative cell volumes at TE (indicated by circle)

Dynamic remeshing within *Fluent* requires a timestep significantly smaller than desirable for the purposes of this project. Testing has found that a minimum of 7000 timesteps per cycle is needed, as opposed to the 500 used in the propulsive case. It was also found that software issues within *Fluent 14.5* mean that solution calculation in parallel among a number of cores is not possible with the use of dynamic remeshing for this type of mesh. This has created computational times of well in advance of one week per cycle.

Unlike smoothing, remeshing does not preserve the boundary layer mesh by bringing the near mesh with the airfoil. Instead all cells are considered fixed. In order to maintain mesh quality the entire path of the airfoil motion must be cell dense. Since the airfoil path is in the order of metres, the number of elements in the mesh may be extreme and thus computational expensive. Therefore in an effort to maximise mesh quality and minimise computational time, the setup depicted by Figure 7 was chosen.

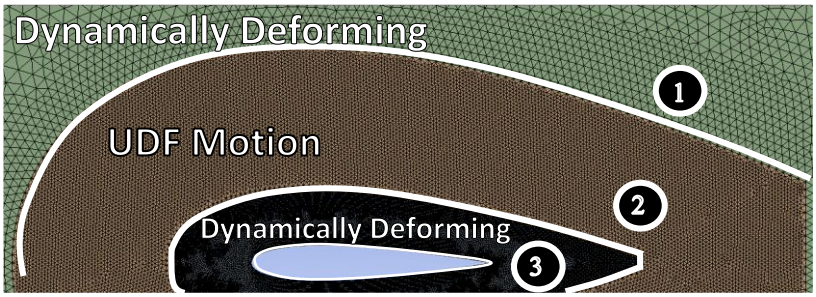

Figure 7 – Power Extraction Mesh Setup

By applying prescibed grid motion to section 2 of the mesh, we can achieve the same effect as smoothing, by moving the mesh around the arfoil with the airfoil's movement. The mesh movement is achieved through a User Defined Function (UDF) using the same equations of motion specified in Equations 1 &2. This has the added effect of splitting the airfoils movement into two different motions; prescribed motion and pressure deformation. The prescribed motion of the airfoil is no longer carried out by the airfoil's boundary layer mesh (section 3), but is carried out section 1, allowing the airfoil's prescribed motion to be sent to larger cells. Since with dynamic remeshing, the largest timestep allowable is approximately one cell length, a much larger timestep is achieved since the cell size at the section 1 and 2 boundary is approximately ten times as large as the cells on the airfoil's surface. Aerodynamic deformation is still carried out by the boundary layer of the airfoil (section 3 of the mesh), but since the deformation under load is small in comparison to the displacement of the airfoil as a whole, there are minimal negative effects.

C. Structural Solver

Both the motion of the of the airfoil and its deformation under aerodynamic load is calculated by the structural solver. The motion of the airfoil is applied to the airfoil through an external element known as a motion driver. The motion driver, labelled in Figure 8, is a cylinder external to the airfoil at which the motion of the airfoil is applied. The motion driver can be thought of as a hand crank for the airfoil. The motion driver and pivot are specified as rigid, whilst the airfoil body is specified as deformable. The Young's Modulus (E) of airfoil is adjusted in order to acheieve different levels of flexibility. This is further explained in the next section of this report.

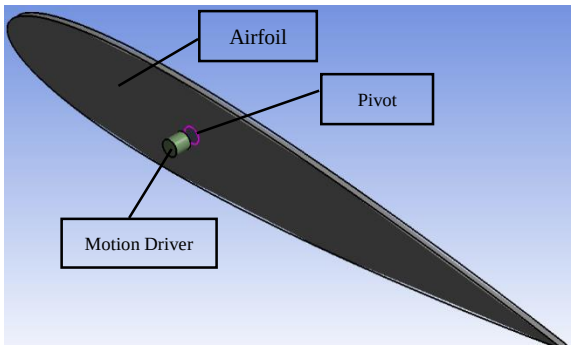

Figure 8 – Structural Setup

The structural side mesh is limited only by the fact that nodes along the FSI interface must physically align with the fluid side mesh in order to adequately link information from both of the solvers. A structural mesh of roughly 10,000 nodes is adequate to minimise computational time and correctly determine airfoil deformation.

D. Flexibility

As previously described, the method of varying airfoil flexibility chosen was through the adjustment of Young's Modulus. Young's Modulus (E) also known as elastic modulus, is a measure of the ratio of axial stress to strain of a material in the plastic (linear) deforming region upon which Hooke's law is valid. Young's Modulus has the units of *Pascals [Pa]* and is most commonly used as a measure of both the stiffness and rigidity. Young's Modulus can be used as a measurable variable for the change of flexibility by the airfoil. It must be noted that flexibility is what the study aims to adjust not specifically Young's Modulus. Young's Modulus just allows the easy adjustment of the flexibility parameter. For the purpose of this work a reduction in Young's Modulus is said to have increased the airfoil's flexibility.

By adjusting the Young's Modulus of a particular material and leaving all other material properties constant, we can feasibly change the material's flexibility. The chosen material of structural steel normally has a Young's Modulus of 2.11e11. All properties of the steel were held constant except for its Young's Modulus. By decreasing the Young's Modulus, the steel was found to significantly deform under both the inertial and aerodynamic loads that it experiences within a flapping cycle. In order to attain a series of Young's Modulus values that would significantly alter the aeroelastic deformation between cases, the Young's Modulus of the structural steel was decreased by a factor of 10 until changes in airfoil shape were noticeable. Note that the amount of deformation is specific to the case type (propulsive or power extraction) so Young's Modulus values that produce significant flexure for the propulsive case may produce insignificant flexure for the power extraction case since the inertial load of the cycle produces the biggest deformation amounts. Young's Modulus values of between 2e11 and 1e6 were found to have no noticeable impact on airfoil flexure or flow structure, whilst values less than E=8e4 deformed the airfoil beyond useful measure and recognition. Thus the range of E=1e5 and 10e5 was used for propulsive cases within this project.

E. Convergence

The solution is deemed to have converge when each coupling iteration has a residual of 10^{-3}. Within each coupling iteration *Fluent* converges at a residual level of 10^{-6} and the structural solver will similarly converge at 10^{-6}. On average the system takes three coupling iterations to converge each timestep. This means that on average the fluid and structural solver has to achieve convergence three times per timestep which equates to large computational times when compared to traditional methods such as ones used by Hoke *et al.* [2]. It should be noted that the more flexibility induced in the airfoil, the more structural iterations that are required for convergence and hence more coupling iterations required.

V. Validation

A grid and timestep independence study was undertaken to determine the solution dependence on both timestep and grid quality for the propulsive case only. No power extraction cases were ran to result extraction level within this project due to time restraints. The independence studies were undertaken using the rigid airfoil propulsive case as defined by Table 1 and 2. Propulsive efficiency was chosen as the performance measure for both the grid and timestep independence studies as described in Part III of this report. Data from the grid and timestep

independence studies were compared to data taken from Maio *et al.* [8] and Hoke *et al.* [2] for the same case in order to validate the solution case.

Grid	Nodes	Airfoil Points per side	Average Y+	Propulsive Efficiency [%]
Coarse	100,000	562	2	22.60
Medium	180,000	1125	1	21.97
Fine	300,000	2250	0.56	21.71

Table 1

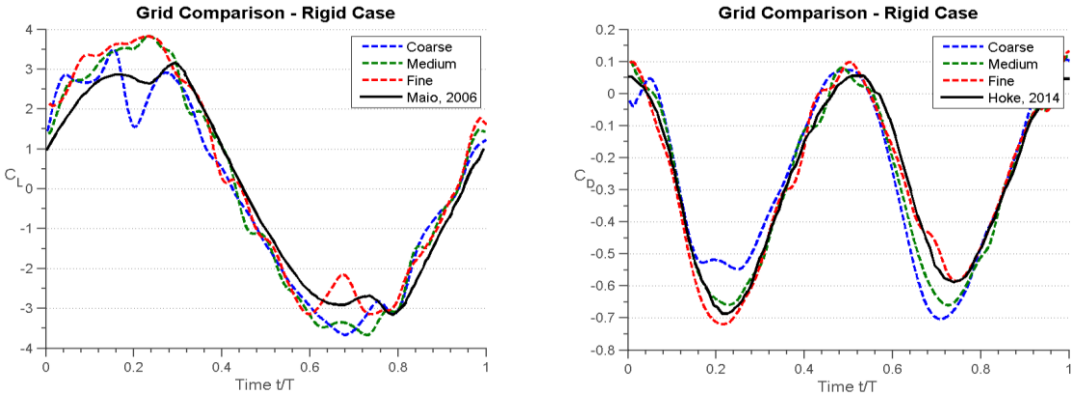

Figure 9 – Grid Independence Study (with Maio et al [8] and Hoke et al [2] case data comparison)

Grid	Timesteps/cycle	Propulsive Efficiency [%]
Medium	500	21.97
Medium	1000	21.61
Medium	2000	21.67

Table 2

From these refinement studies we can see that there is still variation with both increase in timestep and grid quality. It can be shown that there is a 1.2 percent error between the fine and medium mesh and a 1.3 percent error between 500 timesteps per cycle and 2000 timesteps per cycle. While these errors are small, there are noticeable differences between the results of both Hoke and Maio of the same case. This suggests that mesh quality may not be high enough. Hoke *et al.* [2] found propulsive efficiencies of just over 16% for their propulsive case. That means there is roughly 6 percent error in the results of this project. Ideally, a finer mesh and a smaller timestep should be used, however due to time constraints a timestep of 500 per cycle and the medium mesh were deemed appropriate. While 6 percent error is sizeable, variation between grid quality and timestep size is small, which allows for results attained within this project to be deemed accurate when comparing against one another. Thus any performance increases found are still valid.

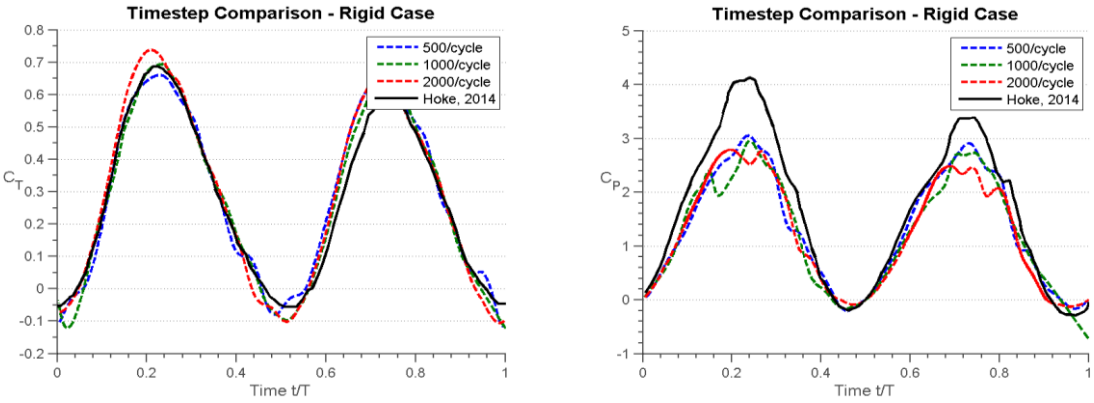

Figure 10 – Timestep Independence Study (with Hoke et al [2] case data comparison)

The largest differences can be seen in the coefficient of power curves (Figure 10). Coefficient of power as stated earlier is calculated using a combination of the coefficient of lift curves and the vertical velocity of the airfoil at that instant. Whilst there is some difference in the C_L curves as shown in Figure 9, there is noticeably more error in the C_P curve. The error therefore is a result of the difference in the vertical velocity equation used compared to the comparative, external data of Hoke *et al.* In this propulsive case for this study, reduced frequency (k) was equal to omega ($2\pi f^*$) as a freestream velocity of 1m/s was chosen. This was not the case for Hoke *et al.*, hence

the velocity equation used was different and hence the error in comparison to this data. This may also account for the 6 percent error found earlier.

VI. Results

As described in Part III, propulsive efficiency is the most convenient and useful data point for the comparison of the net effects of changes in flexibility of the airfoil. Propulsive efficiency as derived in Equation 8 is time averaged thrust over time averaged power. Figure 11 shows how both of these values change with decrease in Young's Modulus. The time averaged force coefficient for the rigid case (Young's modulus of 2e11) is represented on the graph by the black line since its location is well off the right side of the graph. Therefore all data points above the rigid case line are indicative of an increased time averaged force coefficient with increased flexibility.

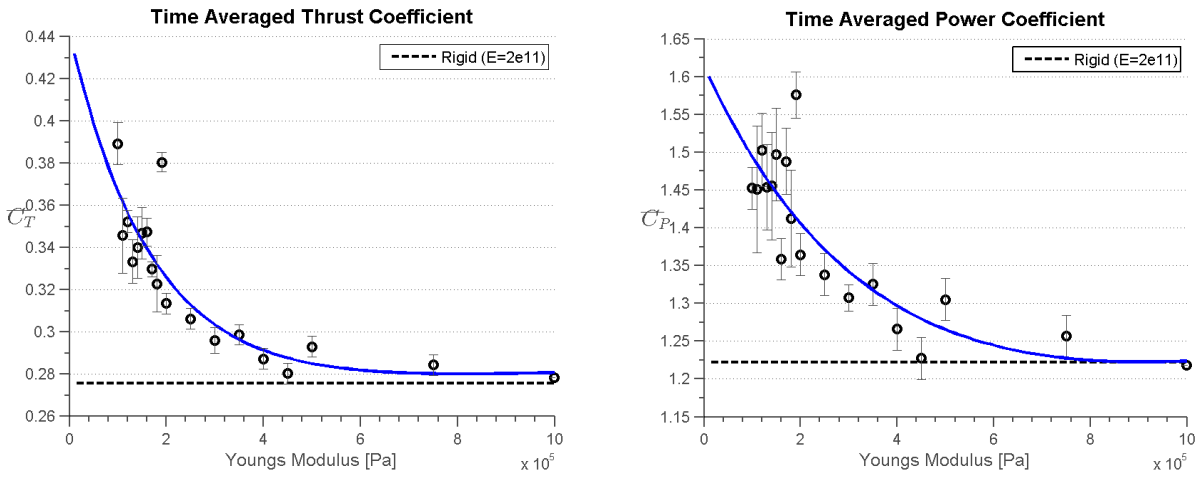

Figure 11 – Time Averaged Force Coefficients

The blue line indicates a line of best fit. The line expresses the data with a Sum of Squares Error (SSE) of 0.4% and 5.2% for the thrust and power coefficient respectively. Both of these error values are small enough to indicate a good fit. The error bars on each curve are representative of the standard deviation of each point on the graph. Each point on the graph is the average of the each force coefficient over a number of cycles. If a particular case was sensitive in outputted values with each cycle, a large error bar is evident. This error source is further explained at the end of this section. Some cases prove much more variable with each cycle. Whilst the line of best fit does not go through all of the error regions on the graph, the error residuals such as SSE and Root Mean Square Error (RSME) calculated for the curve indicate that it is a good fit for the data provided.

Figure 12 shows the propulsive efficiency of the airfoil as the airfoil increases in flexibility. The line of best fit in this case was calculated by dividing the two curves produced in Figure 11 above. Using the relatively low error curves already produced, we derive a more realistic curve fit than otherwise would have been produced through curve fitting by dividing the thrust curve by the power curve as is Equation 8. As is evident, the propulsive efficiency of a flexible, flapping, propulsive airfoil follows an exponential relations which with increased flexibility. Efficiencies of the flexible materials were shown to produce efficiencies roughly 5% higher than the rigid case. Young's Modulus's of less than 1e5 were not assessed since the amount of deformation within each timestep is too large for a smoothing only solution. For E<1e5, remeshing will be required to provide accurate solutions.

Looking at the difference between the rigid case and any flexible case force coefficient curves, it is possible to determine why we see these performance increases. Figure 13 compares the rigid case with the flexible case of E=1e5. Figure 13 A) shows that the flexible airfoil creates much higher peak lift forces at t/T=0.2 than the rigid airfoil. It also creates negative drag (thrust) forces which are almost exclusively higher than the rigid case throughout the whole cycle. At t/T=0.1 Figure 13 A) shows that the flexible airfoil experiences a negative camber due to deformation about the airfoil's pivot center. This camber greatly increases the physical and perceived strength of the existing Leading Edge Vortex (LEV) that was created from the upwards stroke of the previous cycle. The deformed airfoil sucks the LEV closer to the airfoil centerline thus increasing its strength through further decreasing its pressure as well as increasing its perceived strength by reducing the distance between the two structures. The increased size and proximity of the LEV accounts for the large spikes in lift and thus power coefficients at t/T=0.2. The airfoil at the start, midway point and end of each cycle experiences the highest

acceleration due to the airfoil's change in directions. This is evident in Figure 14 B). The acceleration induced inertial load of a flapping, propulsive airfoil therefore produces favorable flow characteristics that aid the increase in propulsive efficiency. The airfoil bends about the pivot located at the one-third chord of the airfoil.

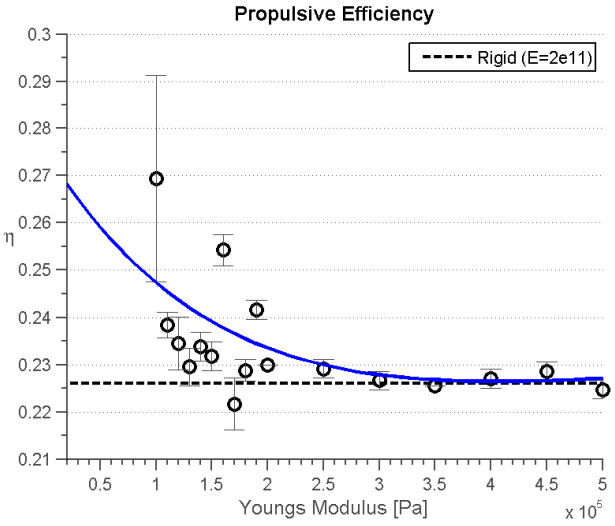

Figure 12 – Propulsive efficiency

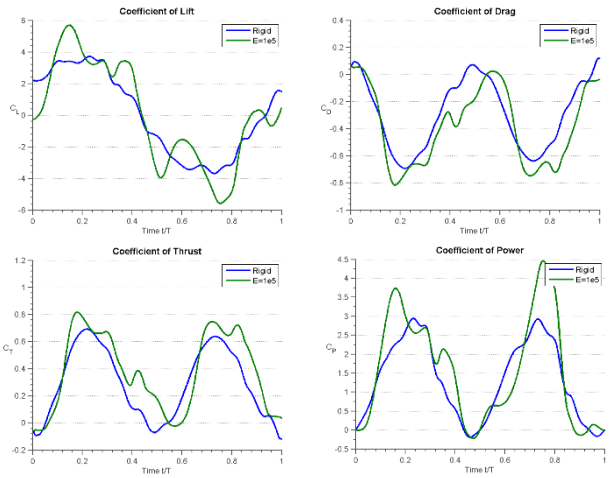

Figure 13 – Rigid (blue) vs Flexible [E=1e5] (Green) Comparison A) Lift B) Drag C) Thrust D) Power

Similarly to the LEV altered at t/T=0.1, a larger and stronger LEV is created at t/T=0.25 on the downward stroke of the airfoil due to a positive angle of attack induced by airfoil deformation. While the pivot of the airfoil cannot rotate, the airfoil body twists around it, allowing the airfoil to have an effective positive angle of attack. This angle of attack causes the large lift and power spike at t/T=0.4 as shown by Figure 13 A). A positive angle of attack is also created during the upward motion of the airfoil. The camber created at the bottom and top of the airfoil's path and the positive angle of attack on its downward and upward motion account for the major changes in LEV flow structure for the flexible cases. The larger LEVs produce higher drag/thrust forces than in the rigid case, through increased LEV interaction with the trailing edge of the airfoil, due to both their size and closer proximity. These two interactions bring about larger thrust forces at nearly every point in the cycle, whilst the lift forces fluctuate but remain fairly constant on average with the values of the rigid case. This inequality of time averaged thrust and power coefficients bring about significant increases of propulsive efficiency as the flexibility of the airfoil is increased. It is worth noting while this is an explanation of the downward stroke, similar events occur on the upwards stroke which also aid in the increase of propulsive efficiency.

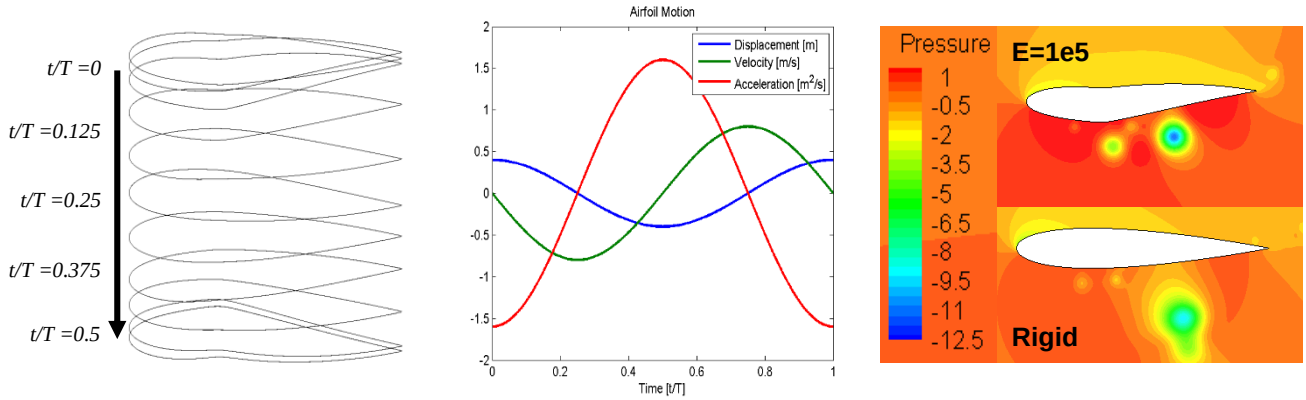

Figure 14 – A) Flexible airfoil deformation B) Airfoil Motion C) Flow Structure & Airfoil Deformation at t/T=0.1

One of the larger problems with the setup used in this project and hence one of the largest sources of error is caused by differences in the airfoil's position between each cycle. Figure 15 shows a cycle comparison of a flexible airfoil case (E=2e5). Whereas for a rigid flapping case, cycle lines will converge on a specific curve, a flexible airfoil shows no possibility of converging between cycles. Figure 15 shows that the starting lift coefficient value in each cycle can vary by up to 3 for this particular case. This effect is due to flutter of the trailing edge, most notably at the end top and bottom of the airfoil's flight path. As the airfoil starts with its trailing edge at a different position for each cycle, invariably the entire cycle's data will significantly differ from cycle to cycle. This leads to problems when assessing results, as the lift and drag forces can be greatly different. As expected, the more flexible the airfoil the more significant the differences between airfoil deformation between each cycle. This is

exemplified in the error bars in Figures 11 & 12 which show that in the most flexible cases, the standard deviation (error bar size) is the largest.

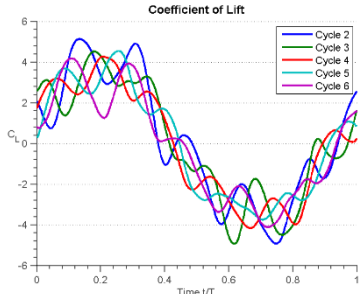

Figure 15 –C_L variability between cycles of a flexible case (E=2e5)

VII. Conclusion

This project has enabled the enabled the study of flexibility on flapping airfoil performance through the use of Fluid Structure Interaction using the *ANSYS* product range. A method was developed in order to allow the three-dimensional testing of a pitching, plunging airfoil for both power extraction and propulsion. Through the use of Finite Element Analysis and Computational Fluid Dynamics software linking, the aeroelastic deformation of an airfoil under both aerodynamic and inertial loads was found able to be calculated throughout a flapping cycle.

The method produced works around some significant issues that were found in the software packages used, thus enabling the simulation of a flapping airfoil with both large vertical and rotational prescribed motion and large and varied aeroelastic deformation. The process involves a quasi-two-dimensional setup that enables adequate comparison to work completed by others in the field such as Kinsey and Dumas [5], Maio et al [8] and Hoke et al [2]. The process has proven to yield comparably similar results to people in the field however time limitations brought about by the nature of this course have not allowed for the smaller timesteps and finer meshes that would have brought about closer and more accurate results. The results produced nevertheless are invaluable in enabling insight into the effects flexibility on flapping efficiency.

Results from this project have shown invariably that for flapping wing propulsion, an increase in flexibility of the airfoil body increases the propulsive efficiency of the airfoil in an exponential fashion. The inertial loads at the top and bottom of the cycle result in the airfoil bending about the pivot location, inducing a camber in the airfoil (negative camber at the top and positive at the bottom), thus resulting in the strengthening of the Leading Edge Vorticy (LEV) that was created earlier by the vertical motion of the airfoil. The strengthening is caused by a suction effect by the airfoil as the trailing edge moves away from its equilibrium position. On the upwards and downwards strokes of the airfoil, a positive angle of attack is created by the aerodynamic load that the airfoil experiences. This has the effect of creating the LEV earlier and larger than would otherwise be seen in the rigid case. These two interactions bring about larger thrust forces at nearly every point in the cycle, whilst the lift forces fluctuate but remain on average fairly similar to those of the rigid case. This inequality of time averaged thrust and power coefficients bring about significant increases of propulsive efficiency as the flexibility of the airfoil is increased.

VIII. Recommendations

The largest part of this project surrounded the development and implementation of the methodology that is used to allow the simulation of a pitching, plunging airfoil using Fluid Structure Interaction for power extraction. Results were only attained for a propulsive regime of a flapping airfoil due to time restrictions associated with the nature of this course. The propulsive case proved easier to setup and invariably quicker to run, and thus was brought within the scope of the project.

The simulation of a power extraction case has been outlined within this report and thus a future project would need to focus more on attaining results and looking more closely at the complex flow structures that surround a flapping wing airfoil than that which was covered within the scope of this project. The updating of the method from *ANSYS v14.5* to *ANSYS v15.0* or later would also prove invaluable due to supposed software fixes that would allow the simulations to run more efficiently.

Acknowledgements

Sincerest of thanks to Mr. Charles Hoke for his guidance and mentoring throughout the duration of this project, and for his hard work in the role of my thesis supervisor. Also many thanks to Mr. Vishal Naidu for his patient technical direction on some of the more difficult areas of the solution setup, without which this project would have stalled prematurely.

References

[1] Ashraf, Isaacs, Young, Lai, Ray. 2009. "Numerical Simulation and multiobjective design of flow over oscillating airfoil for power extraction." *14th International Conference of modelling fluid flow technologies.* Budapest, Hungary.

[2] Hoke, Young, Lai. "Time-Varying Deformation Shape Effects on Flapping Foil Propulsion and Power Extraction." *Under review for Journal of Fluids and Structures*

[3] Hoke, Young, Lai. 2014. "Time-Varying Flexible Airfoil Shape Effects on a Flapping Airfoil Power Extraction." *32nd ASME Wind Energy Symposium, 2014, 10.2514/6.2014-1217*

[4] Kinsey, Dumas. 2012. "Optimal tandem configuration for oscillating-foils." *Journal of Fluids, Vol 134, No 3.*

[5] Kinsey, Dumas. 2008. "Parametric Study of an Oscillating Airfoil in a Power-Extraction Regime." *AIAA Journal, Vol 46, No 6.*

[6] Le, Ko, Byun. 2013. "Morphological effect of a scallop shell on a flapping-type tidal stream generator." *Bioinspiration and Biometrics, Vol 8, No 3* 036009.

[7] Liu, Xiao, Cheng. 2013. "A bio-inspired study on tidal eneregy extraction with flexible flapping wings." *Bioinspiration and Biometrics, Vol 8.*

[8] Maio, Ho. 2005. "Effect of Flexure on Aerodynamic Propulsive Efficiency of Flapping Flexible Airfoil." *Journal of Fluids and Structures.*

[9] McKinney, DeLaurier. 1981. "The Wingmill: An Oscillating-Wing Windmill." *Journal of Energy, Vol 5, No 2* 1318-1330.

[10] Young, Lai, Platzer. 2014. "A Review of Progress and Challenges in Flapping Foil Power Generation." *Progress In Aerospace Sciences.*